Advanced Composites and Hybrid Materials (2025) 8:312
https://doi.org/10.1007/s42114-025-01345-7

RESEARCH

Chromium (VI) remediation via biochar@polyaniline composite: advancing water treatment using biogas residue digestate

Ayoub Chaoui[1] · Abdelaziz Imgharn[1] · Ana C. Estrada[2] · Aboubakr Ben Hamou[1] · Salaheddine Farsad[1] · Nisrine Nouj[1] · Mohamed Ez-zahery[1] · Tito Trindade[2] · Abdallah Albourine[1] · Noureddine El Alem[1]

Received: 9 October 2024 / Revised: 3 May 2025 / Accepted: 23 May 2025

Abstract
The demand for effective water treatment strategies has contributed for extensive research in materials chemistry, with great focus on advancing adsorbent technologies. This investigation centers on synthesizing and modifying carbonaceous materials, specifically biochar and its polyaniline composite (biochar@polyaniline: BC@PANI), to evaluate their effectiveness in eliminating hexavalent chromium Cr(VI) from aqueous solutions. The biochar composite was prepared using a straightforward in-situ chemical polymerization approach. The properties of biochar were modified by blending it with polyaniline at 25%, 50%, and 75% (w/w), successfully loaded into the biochar samples. For elucidating structural changes and functionalities introduced during modification, the synthesized materials were fully characterized using different techniques. The adsorption performance of BC@PANI50% was systematically evaluated through batch adsorption experiments. This PANI-modified biochar material exhibited exceptional adsorption capacity for Cr(VI) removal from aqueous samples, reaching 877.19 mg/g at 318.15 K, emphasizing its potential for water adsorption treatments. Our research in the kinetics of Cr(VI) removal showed that both pseudo-second-order and Langmuir models adequately described the adsorption process. Regeneration experiments demonstrated that, even after undergoing five cycles, BC@PANI showed 82.5% Cr(VI) removal indicating its exceptional reusability and stability. In summary, this study establishes the potential applicability of BC@PANI adsorption for the removal of Cr(VI) ions in water, providing a promising avenue for integrating such sorbents into water treatment engineering practices.

Keywords Biogas residue · Cr(VI) adsorption · Composites · PANI · Biochar · Regeneration

1 Introduction

Environmental pollution is a global threat negatively impacting both human health and ecosystems. Among the several contaminants present in water bodies, hexavalent chromium (Cr(VI)) poses great concern due to its toxic and carcinogenic properties [1]. Acute exposure to Cr(VI) causes several health problems such as kidney failure, liver diseases, lung cancer, ulcer formation and other illnesses [2]. In contrast, Cr(III) is considered less hazardous. Therefore, it is paramount to explore and develop effective approaches that can simultaneously eliminate and reduce Cr(VI) to Cr(III). The maximum permissible concentrations of Cr(VI) oxyanion in drinking water and industrial wastewater are 0.05 and 0.10 mg/L [3, 4]. Hence, Cr(VI) oxyanion-containing wastewater is required to be treated to achieve certain discharge standards. Chemical reduction, electrochemical reduction, photocatalysis reduction processes and so on, are used to tackle Cr(VI)'s threats [5]. While these processes have proven effective, their dependence on high-energy inputs or the utilization of reducing reagents is likely to lead to an increase in operational costs [6]. Sequential Cr(VI) oxyanion reduction-adsorption to Cr(III), followed by its immobilization, is regarded as an alternative approach to decontaminate aqueous systems containing Cr(VI). This strategy presents several advantages, owing to its tunability, easy processing and requires inexpensive adsorbent/reducing materials [7].

✉ Ayoub Chaoui
ayoub.chaoui@edu.uiz.ac.ma

[1] Laboratory of Materials and Environment, Faculty of Sciences, Ibn Zohr University, Agadir, Morocco

[2] Department of Chemistryand, CICECO - Aveiro Institute of Materials, University of Aveiro, 3810-193 Aveiro, Portugal

Published online: 24 July 2025

Recently, biochar materials have gained attention for their potential application in environmental remediation [8], particularly in the adsorption of heavy metals from contaminated water [9, 10]. These materials can be produced through the pyrolysis of biomass, such as agricultural residues or woody biomass, in the absence of oxygen [11–13]. Their porous structure and high specific surface area make them effective adsorbents for a range of heavy metal ions [14].

Digestate is the complex mixture that remains after anaerobic digestion of organic matter. Also known as biogas residue, digestate has gained increasing attention for biochar preparation and various other applications. Composed of both organic and inorganic nutrients, digestate can enhance soil fertility and improve its structure and sorption capacity. Due to its high nutrient content, digestate can be effectively used in plant fertilization, serving as a supplement or even a replacement for mineral fertilizers [15, 16]. In addition, the organic matter present in digestate, such as humic acids and proteins, contributes to the renewal of soil organic matter, acting as a soil conditioner that influences the biological, chemical, and physical properties of the soil. The solid fraction of digestate, characterized by reduced water content (generally between 60 and 75%), is particularly suitable as a substrate for the composting process [17, 18]. Furthermore, with a carbon content ranging from approximately 15% to 55%, digestate serves as a potential carbon precursor to produce carbonaceous materials such as biochar. Biochars derived from digestate are attracting growing interest in wastewater treatment, whether through conventional adsorption processes or advanced oxidation processes, such as persulfate activation [19–21].

As environmental standards become more stringent, it has become clear that raw biochar (BC) might not adequately eliminate contaminants when present at high concentrations and may not fulfill the demand for selectively decontaminating pollutants in complex real-world wastewater conditions [22]. To address these limitations, the development of biochar-based composites has gained great interest, aimed at strengthening its overall efficacy [23–25].

In this context, the conjugated polymer polyaniline has been explored as a modifier for biochar for Cr(VI) adsorption, taking advantage on properties such as conductivity, redox activity, and chemical reactivity [26–28]. Polyaniline has redox-active sites that can facilitate the reduction of Cr(VI) to Cr(III), thus leading to an ionic form less mobile and less toxic [27, 29]. This reduction process may also contribute to the removal of anionic Cr(VI) species from aqueous solutions due to favorable electrostatic interactions with N-protonated moieties of functional groups in the polymer [30, 31]. Therefore, PANI-modified biochar has the potential to serve simultaneously as an adsorbent and reducing agent for anionic Cr(VI) contaminants dissolved in water.

Herein, biochar sorbents containing various amounts of PANI have been engineered to adsorb/reduce Cr(VI) present in water samples. A systematic study was carried out to investigate the effect of several experimental parameters (e.g. temperature, adsorbent dose, pH). and the selectivity on the Cr(VI) elimination. Finally, the regeneration of BC5@PANI composite was conducted to evaluate its inexhaustibility and stability.

2 Materials and methods

2.1 Chemicals

The materials employed in this study include: aniline monomer, 1,5-diphenylcarbazide, nitric acid (HNO_3), hydrochloric acid (HCl), phosphoric acid (H_3PO_4), sulfuric acid (H_2SO_4), sodium sulfate (Na_2SO_4), sodium hydroxide (NaOH), acetone (C_3H_6O), and potassium dichromate ($K_2Cr_2O_7$), all of which were supplied by Sigma-Aldrich. Additionally, distilled water was used consistently throughout the research.

2.2 BC@PANI Preparation

- BC Preparation

Our earlier research thoroughly delineated the process of preparing the activated biochar employed in this study [32]. Briefly, the poultry by-product digestate resulting from the methanation process underwent a series of meticulously detailed steps. Initially, the digestate was dried at 105 °C, followed by multiple washes with distilled water and subsequent grinding. The resulting material was then pyrolyzed at 500 °C for 3 h, resulting in a biochar product, which was crushed and sifted through a 50 µm sieve. This biochar was subsequently activated through treatment with 2 M HNO_3 in a 50:1 (V/W) ratio for 12 h under continuous stirring at 25 °C. The resulting mixture was filtered, and the residue underwent multiple washes with distilled water until a neutral pH was achieved. Finally, the resulting biochar was dried and crushed to achieve the desired physical characteristics for subsequent modification.

- Preparation of BC@PANI composite

The in-situ oxidative polymerization of an aniline monomer was used to prepare BC@PANI composites containing a varying amount of PANI (25, 50 and 75% w/w). Typically, a BC@PANI50% sample was prepared by

adding 1 g of BC into a 50 ml solution of 0.1 M HCl (Solution A), and the mixture was vigorously shaken for ½ hour. Subsequently, 0.5 mL of aniline was added to the solution, followed by a stirring period of 3 h. Meanwhile, in a separate vessel, Solution B comprising 2.62 g of sodium persulfate dissolved in 50 ml of 0.1 M HCl was vigorously agitated for ½ hour. The resultant Solution B was then gradually added dropwise to Solution A under continuous stirring, leading to an immediate color transformation from black to dark green, indicative of the ongoing oxidative polymerization process. The mixture was left to stir for an additional 12 h at room temperature. The resulting residue underwent filtration, followed by multiple washes with distilled water and acetone to remove any remaining oligoaniline and excess of oxidant, and finally was dried at 80 °C. The ensuing product of the chemical synthesis was the composite labeled as BC@PANI50%. The same procedure was followed to synthesize the composite samples BC@PANI25% and BC@PANI75%. Figure 1 summarizes the overall process to produce the BC@PANI composites.

2.3 Characterization Techniques

FTIR spectra with attenuated total reflectance (ATR) were collected using a Bruker Tensor 27 spectrometer, with a resolution of 4 cm^{-1} and 256 scans. Powder X-ray diffraction (DRX) data were collected using a PANalytical Empyrean X-ray diffractometer equipped with a monochromatic Cu Kα radiation source at 45 kV/40 mA. Raman spectra were measured using a Bruker MultiRAM FT-Raman spectrometer equipped with a Nd:YAG 1064 nm laser. In addition to SEM micrographs, elemental analyses of the gold-coated samples were conducted using a JED Model 2300 energy dispersive X-ray analyzer and an accelerating voltage of 15 kV. A N2 adsorption–desorption method was used to analyze surface area on an automated surface area analyzer (Micromeritics Gemini 2380).

2.4 Adsorption experiments

In the execution of batch adsorption experiments, the ambient temperature was carefully regulated, except for instances involving temperature-dependent investigations, which were conducted on a water bath shaker operating at 175 r/min. To assess the influence of pH, experiments were undertaken across a range of values (pH 2–10) using a 20 ml solution containing Cr(VI) at a concentration of 100 mg/L. An adsorbent dosage of 0.75 g/l was applied, and the solution's pH was meticulously adjusted utilizing 0.1 M HCl and NaOH. Diverse adsorbent dosages (0.125 to 1.5) were systematically introduced into distinct 50 ml Cr(VI) solutions (100 mg/L) at pH 2. These experiments were strategically designed to probe the adsorption process under varying conditions. Adsorption isotherm data were meticulously acquired at temperatures of 298, 308, and 318 K, employing a thermostatic water bath shaker set at 175 rpm. Initial Cr(VI) concentrations spanned from 100 to 1000 mg/l, accompanied by a solid loading of 0.75 g/L. Samples were extracted at predetermined intervals and subjected to filtration through a 0.45 µm membrane filter. Post-experimentation, the residual concentrations of Cr(VI) ions were precisely determined through complexation methods utilizing 1,5-diphenylcarbazide. Subsequent analysis involved a UV2300 spectrophotometer, measuring the absorbance at the maximum wavelength of 540 nm. All the experiments were performed at least in duplicate. Thermodynamic investigation was conducted at three temperatures (298, 308, and 318 K) to gain a deeper understanding of the underlying energy interactions and spontaneity of the process. A summary of the equations used in this study can be found in Table S1.

An acidified potassium permanganate solution was used to completely oxidize the Cr(III) ions in the filtrate solutions to determine the total chromium content after the adsorption experiments. As described above, total chromium concentration (equal to Cr(VI) concentration) was quantified by UV–vis absorption. In order to find the Cr(III) concentration, the Cr(VI) concentration was subtracted from the total chromium concentration [7, 33].

2.5 BC@PANI regeneration and desorption

The regeneration experiment spanned 6 h, employing a 1 M NaOH eluent solution to facilitate the desorption of Cr(VI) ions from BC@PANI composite. The successful regeneration process involved thorough washing of the BC@PANI composite with distilled water, followed by treatment with 1 M HCl to prepare the sample for an additional adsorption cycle. The regeneration potential of BC@PANI was conducted through a total of five consecutive adsorption/desorption cycles.

3 Results and Discussion

3.1 Characterization of the BC@PANI composites

3.1.1 Powder XRD

Powder XRD analysis was conducted to elucidate about the crystalline domains in the activated biochar, before and after modification with polyaniline (PANI) at the varying percentages (25%, 50%, and 75%) investigated in this research. As depicted in Fig. S1, the XRD patterns of the activated biochar features distinctive peaks of graphitic carbon at 2θ values of 26.6° and 60.0°. Additionally, the XRD analysis

also indicated the presence of quartz as a crystalline component in the biochar samples, as assigned by the characteristic peaks at 2θ values 20.9°, 26.6°, 36.5°, 39.5°, 42.4°, 50.1°, and 68.2°. After PANI modification, the XRD pattern analysis provided a first indication for the successful modification of activated biochar through the incorporation of polyaniline (PANI). In fact, the analysis of the XRD patterns reveals that as the percentage of PANI in the samples increases, there is a decrease in the intensity of the characteristic peaks of the activated biochar. This attenuation in peak intensity is indicative of an increased disorder in the crystallinity of the biochar, attributable to the amorphous structure introduced by PANI. The increasing amount of PANI in the composites disrupts the ordered arrangement of the biochar's crystalline lattice, leading to a decrease in peak intensities. This is an indication of the structural modification of activated biochar after PANI incorporation, thus reinforcing the amorphous nature imparted by the polymer. Similar trends have been reported for the modification of tungsten trioxide (WO_3) with polyaniline [34].

3.1.2 FTIR spectroscopy

The FTIR analysis provides information on the transformation of biochar, both pre- and post-modification, incorporating various polyaniline (PANI) percentages (25%, 50%, and 75%). This analysis is particularly relevant for understanding how these modifications on the chemical composition of biochar impact on Cr(VI) ion adsorption. The FTIR spectra in Fig. 2 show changes on the characteristic vibrational bands induced by PANI modification, pinpointing specific functional groups that might be involved in the adsorption process. The FTIR spectrum of biochar is also shown for comparison. Characteristic vibrational features include a broad band (3600–3000 cm^{-1}) attributed to -OH stretching [35], aromatic C = C stretching at 1599 cm^{-1} and pronounced bands indicative of carbonyl groups at 1534 cm^{-1} [36, 37]. The -C-O band of the carboxylic functional groups present in aryl ethers is located at 1018 cm^{-1} [38, 39]. Following PANI modification, the FTIR spectra show several changes, which is mostly evident by the vibrational bands at 1583 and 1534 cm^{-1}. These bands are assigned to the stretching modes of C = C in quinonoid and benzenoid units of PANI chains [34, 40], respectively. Furthermore, the sharpness of the band assigned to the benzenoid unit increased with the percentage of PANI loaded on biochar. Additionally, the band shown at 1313 cm^{-1} intensifies in tandem with higher PANI percentages, aligning with the -C-N stretching vibration of aromatic amine [28]. Simultaneously, the band at 1140 cm^{-1} corresponds to the in-plane bending vibration attributed to -C-H bonds in benzenoid or quinonoid structures [41]. This observation substantiates the successful modification of biochar by polyaniline. After Cr(VI) adsorption, the location of vibrational bands characteristic of the BC@PANI composite exhibited noticeable changes. Some bands shifted significantly, new bands emerged, and the intensity of other spectral bands varied to different degrees. The bands corresponding to the C = C and C = O groups, originally located at 1564 cm^{-1} and 1485 cm^{-1}, shifted to 1578 cm^{-1} and 1493 cm^{-1}, respectively, as well, the C-H symmetrical bending vibration band at 1294 cm^{-1} shifted to 1304 cm^{-1}. The appearance of the C-H asymmetrical bending vibration band at 1375 cm^{-1} after Cr(VI) adsorption is also noticeable. Furthermore, the bands at 1026 cm^{-1}, 823 cm^{-1}, and 793 cm^{-1} showed a slight shift and increased sharpness after the adsorption of Cr(VI) species. The removal of Cr(VI) by the BC@PANI composite is attributed to the presence of such functional groups that bind to Cr(VI) during the adsorption process.

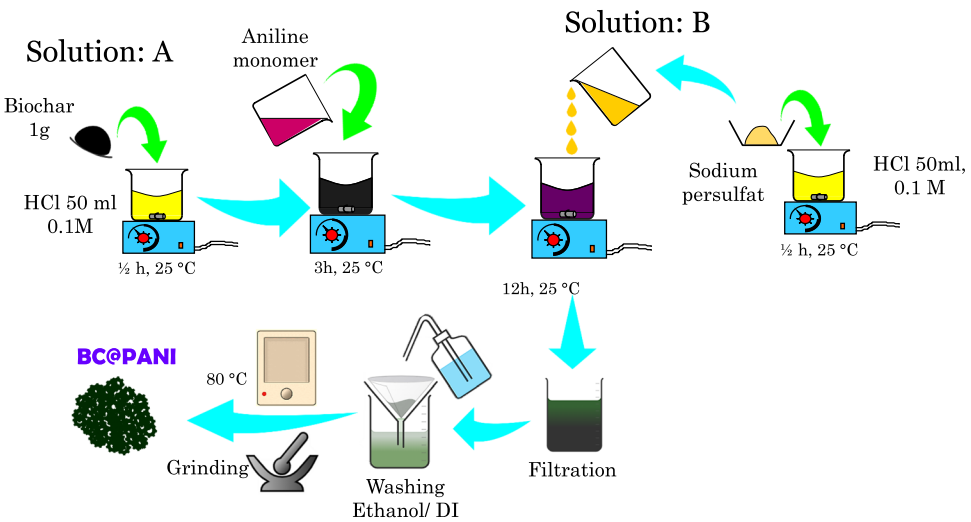

Fig. 1 Scheme of the main steps for preparing the BC@PANI composite samples

3.1.3 Raman spectroscopy

The Raman spectra of both untreated biochar and BC@PANI composite were examined. The Raman bands of the unmodified biochar sample (Fig. 3. a, c) shows the D-band, indicative of structural defects, and the G-band, ascribed to crystalline graphite, at 1324 cm^{-1} and 1595 cm^{-1}, respectively. These spectral features align with the characteristic D- and G-bands of other carbonaceous materials, which have been observed at similar spectral regions [42]. Following the modification of biochar, the Raman spectrum of BC@PANI composite show significant changes in the 300 to 1000 cm^{-1} region. Thus, the vibrational bands observed at 416, 806, and 870 cm^{-1} (Fig. 3.b) are ascribed to the out-of-plane and in-plane vibrational modes of the aromatic rings in the protonated form of PANI (emeraldine structure) [43]. Additionally, the band at 515 cm^{-1} corresponds to the cross-linking between polyaniline chains [44]. As shown in Fig. 3.c, the intense band at 1176 cm^{-1} in the Raman spectrum is attributed to the C-H out-of-plane bending vibrations within benzenoid units and deformation of quinoid units of the polymer chain [7, 44]. The Raman band at 1263 cm^{-1} is ascribed to the C–N stretching of amine groups of PANI [43]. The band at 1371 cm^{-1} is associated with C-$N^{+\bullet}$ stretching vibration modes, indicative of delocalized polaronic charges along the PANI chains [7, 44]. Additionally, the Raman bands around 1506 and 1620 cm^{-1} are ascribed to the C–N stretching mode of the benzenoid ring and the C = C stretching vibration of the quinoid ring, respectively [45]. In brief, the Raman analysis confirms that the biochar has undergone successful modification by polyaniline.

3.1.3.1 SEM/EDS Figure 4 shows the SEM images of the composite samples BC and, BC@PANI before and after Cr(VI) adsorption. The activated biochar (BC) surface displays a homogeneous, etched, and rough texture with a porous structure. After the PANI modification, the BC@PANI composite surface shows a smoother and flatter coating layer, as compared with BC [46, 47]. After the adsorption of Cr(VI) ions, the BC@PANI composite underwent surface modifications as the Cr(VI) ions were uptaken into the structure. As expected, the EDS spectra and elemental mapping images of BC@PANI, before and after Cr(VI) adsorption, reveal changes in the elemental composition. Figure 4 also shows the results for the BC sample, which is mainly composed of carbon, oxygen, and silicon, with mass percentages of 73.97%, 22.93%, and 3.10%, respectively. Following the polyaniline coating on the biochar surface, the EDS spectrum shows the appearance of a nitrogen peak at 0.35 keV with a mass percentage of 3.21%, consistent with the formation of the BC@PANI composite. After Cr(VI) adsorption, as shown in Fig. 4, the EDS spectrum reveals the appearance of two new peaks at 5.4 and 5.9 keV. These peaks confirm that Cr(VI) ions were adsorbed onto the BC@PANI surface, with a mass percentage of 14%. Other have reported similar results for samples modified with o-polyaniline and submitted to adsorption studies involving Cr(VI) species [28, 48].

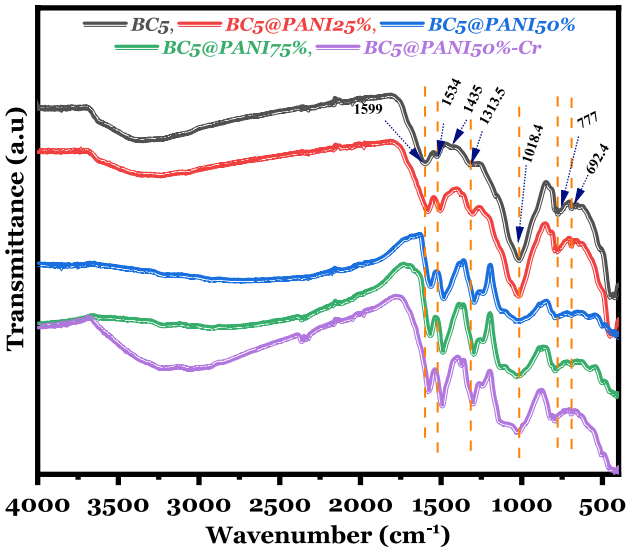

Fig. 2 FTIR spectra of BC5 and BC5@PANI materials with various amounts of PANI, as indicated

3.1.4 BET (Brunauer–Emmett–Teller) adsorption measurements

The porous structure of the prepared biochar, both before and after modification with varying percentages of PANI, was characterized using N_2 adsorption/desorption isotherms. As illustrated in Fig. 5, the adsorption–desorption isotherms of the prepared biochar, both before and after PANI modification, exhibit typical Type IV behavior and are irreversible [49]. As depicted in Table S2, the specific surface area of BC dropped significantly from 39.138 m^2/g to 7.933 m^2/g after the PANI coating was applied. This reduction indicates pore blockage and confirms the successful loading of polyaniline on the biochar surface. Moreover, after PANI modification, the average pore size of BC increased from 95.62 Å to 162.04 Å for BC@PANI75% composite, while the pore volume decreased from 0.0808 cm^3/g to 0.0408 cm^3/g.

3.2 Factors influencing the adsorption

3.2.1 Biochar/PANI ratio

In the investigation of the effect of the biochar to polyaniline (PANI) ratio on Cr(VI) elimination, four distinct materials, including biochar (BC), BC@PANI25%, BC@PANI50%, and BC@PANI75%, were examined through

rigorous Cr(VI) elimination tests. Remarkably, as depicted in Fig. 6.a, the results revealed an intricate relationship between the PANI content and the efficiency of Cr(VI) removal. Notably, an increase in the proportion of PANI up to 50% of the biochar mass prominently enhanced the Cr(VI) elimination rate, with an optimal removal rate of 80.62% achieved. However, upon further escalation of the PANI concentration to 75% of the biochar mass, the removal efficiency exhibited a decline to 72.36%. Furthermore, the data depicted in the figure unambiguously demonstrate the considerable adsorption percentage exhibited by the BC@PANI composite in contrast to the standalone BC (15.75%). This disparity underscores the pronounced synergistic interplay between PANI and activated biochar particles, elucidating their combined efficacy in the adsorption process. Consequently, the BC@PANI50% composite was selected for continued investigation regarding Cr(VI) adsorption, aiming to unravel the specific parameters contributing to heightened adsorption capacity. This choice stems from the dual objective of achieving an optimal chromium (VI) removal rate while minimizing the use of PANI to ensure economic viability in the adsorption process.

3.2.2 Effect of pH

To acquire new insights about the adsorption mechanism of Cr(VI) species on BC@PANI, an extensive examination was carried out to assess how different pH values (2—10) influence the detoxification Cr(VI) oxyanions by the designed material. Considering the established PZC value 2.76 and illustrated in Fig. 6.b, the BC@PANI composite exhibited its highest efficacy in detoxifying Cr(VI) oxyanions under lower pH conditions, specifically below the PZC value. Significantly, the adsorption efficiency for Cr(VI) oxyanions surpassed 95%, reaching a maximum adsorption capacity of 125 mg/g, at pH = 2. However, as pH values increased, the efficacy of Cr(VI) decontamination declined, with only 20.62% of Cr(VI) oxyanions being detoxified at pH = 10. To interpret these findings, it is crucial to take in consideration the diverse forms of Cr(VI) species (e.g. $H_2Cr_2O_7$, $Cr_2O_7^{2-}$, $HCrO_4^-$, CrO_4^{2-} and $HCr_2O_7^-$) present in an aqueous solution within the studied pH range [3]. At pH values below 6, the prevailing species include $HCrO_4^-$ and $Cr_2O_7^{2-}$. A decrease on the solution pH promotes the protonation of amino groups on the BC@PANI composite, leading to the adsorption of $Cr_2O_7^{2-}$ and $HCrO_4^-$ through electrostatic interactions (Eqs. 1 and 2). Henceforth, Cr(VI) undergoes an in situ chemical reduction, by converting into Cr(III) species, as shown by the half-Eqs. 5 and 6 for the reduction components in the redox reactions. Following this reduction, the resulting Cr (III) has the potential to chelate with the nitrogen-containing groups within BC@PANI [50–52], as Eqs. (1–4) depict.

$$-NH_3^+ + HCrO_4^- \rightarrow NH_3^+ - HCrO_4^- \quad (1)$$

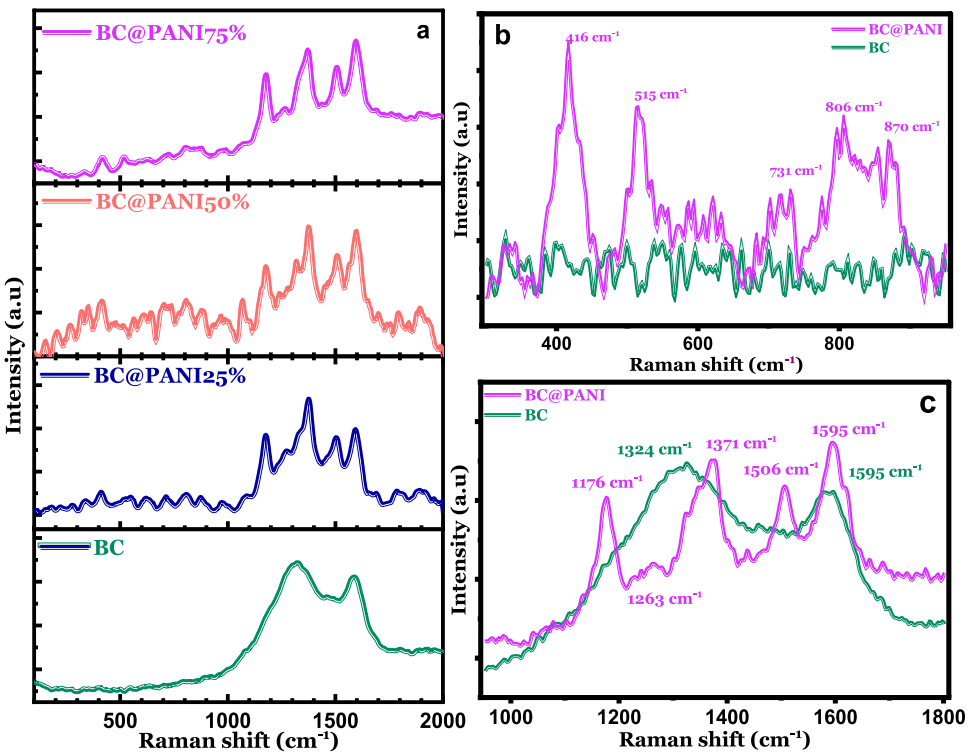

Fig. 3 Raman spectra of BC (a) and BC@PANI materials with various amounts of PANI (b), (c)

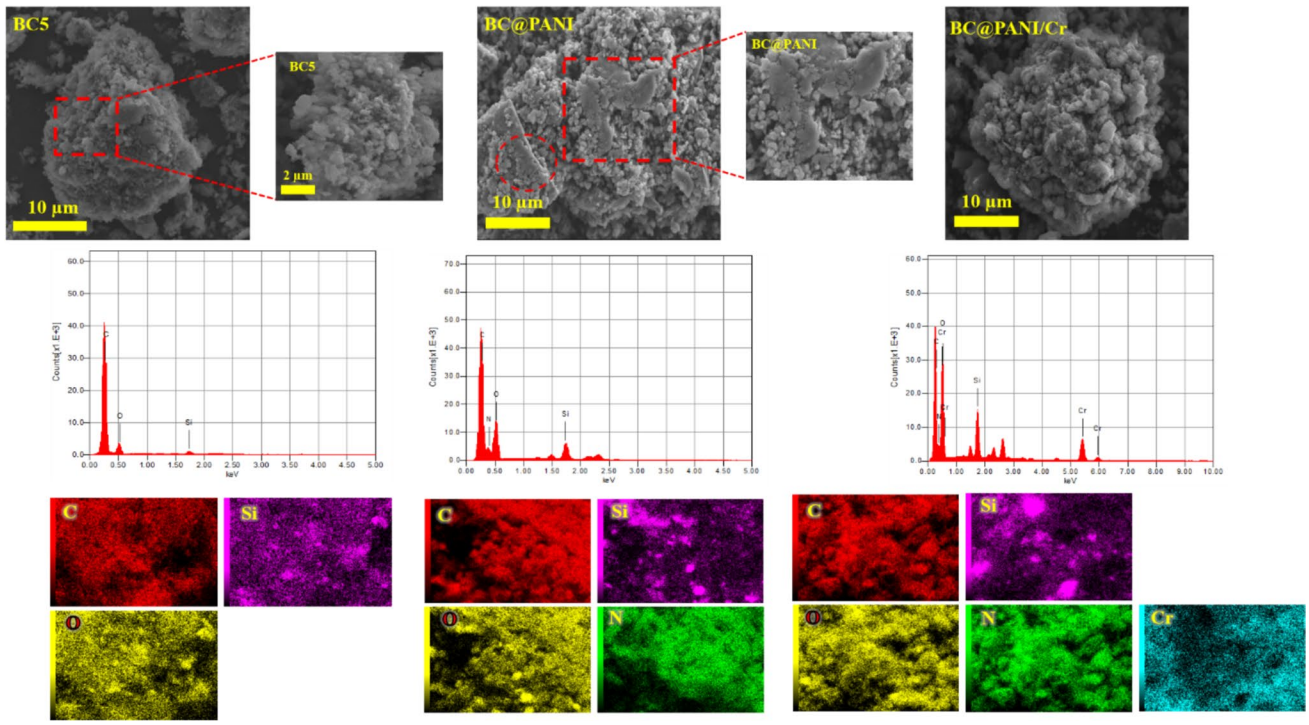

Fig. 4 SEM micrographs of BC5 and, BC@PANI before and after Cr(VI) adsorption, along with the respective EDS elemental spectra and element mapping images

$$-NH_3^+ + Cr_2O_7^{2-} \rightarrow -NH_3^+ - Cr_2O_7^{2-} \quad (2)$$

$$HCrO_4^- + 7H^+ + 3e^- \rightarrow Cr^{3+} + 4H_2O \quad (3)$$

$$Cr_2O_7^{2-} + 14H^+ + 6e^- \rightarrow 2Cr^{3+} + 7H_2O \quad (4)$$

As the solution's pH increased, the deprotonation of the amine group intensified, leading to a weakened electrostatic force between the adsorbent and Cr(VI) (CrO_4^{2-}) oxyanions. This phenomenon resulted in a reduced percentage removal of Cr(VI). Overall, it is unequivocally established that the removal of Cr(VI) is driven by a synergistic mechanism, involving a combination of adsorption and in situ reduction processes.

The total amount of Cr in the filtrate solutions were quantified after adsorption assays and compared to Cr(VI). No Cr(III) species were detected in the solution, indicating no difference between the concentration of Cr(VI) and total Cr in the filtrate. This suggests that the BC@PANI composite effectively immobilize Cr(III), likely due to a large amount of N- and S-containing functional groups on the surface.

3.2.3 Effect of Adsorbent dose

The known relationship between the adsorbent dosage and the residual concentration of Cr(VI) directly influences the overall cost of the adsorption process [52]. To optimize the quantity of BC@PANI used, an investigation into Cr(VI) adsorption was pursued, varying the BC@PANI dose from 0.1 g/L to 1.5 g/L, at pH 2 and ambient temperature. As illustrated in Fig. 6.c, by increasing the amount of BC@PANI in the system, an increase was observed in the removal efficiency of chromium (VI), rapidly increasing to 94.12% with the augmentation of BC@PANI dosage from 0.1 g/L to 0.75 g/L. The significant increase can be ascribed to the direct correlation between the quantity of the adsorbent and the available active sites for Cr(VI) adsorption, wherein augmenting the adsorbent dosage leads to an expanded adsorbent surface area, thereby facilitating the availability of additional binding sites on the surface for the uptake of Cr(VI) species [51, 53]. Beyond this threshold, the removal efficiency revealed a slight elevation before eventually stabilizing or reaching a plateau. This observation highlights the saturation of active sites or the establishment of an equilibrium state, emphasizing the complex dynamics governing the interaction between the dosage of the adsorbent and the efficacy of chromium (VI) removal. Contrarily, the adsorption capacity of BC@PANI composite for Cr(VI) diminishes as the adsorbent dose increases. This decrease may be attributed to particle agglomeration occurring in the dispersed sorbent, wherein an excess of BC@PANI leads to the partial

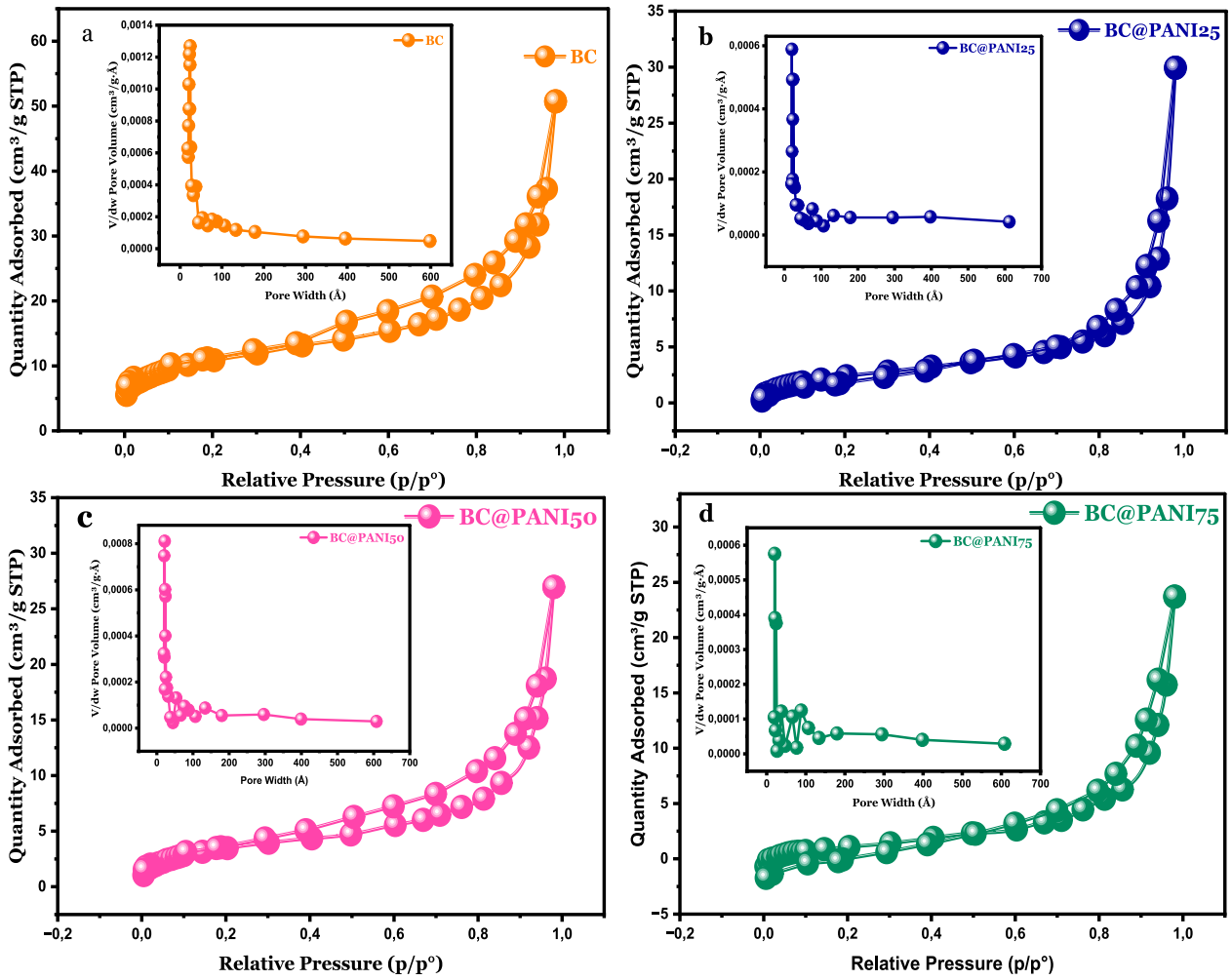

Fig. 5 N_2 adsorption isotherms and pore size distribution of BC5 and BC5@PANI materials with various amounts of PANI **(a-d)**

utilization of the adsorption sites, consequently reducing the adsorption capacity for Cr(VI) [54]. Similar trends in Cr(VI) removal have been noted by other researchers [55, 56].

3.2.4 Effect of contact time

At ambient temperature and a solution pH of 2 for BC@PANI, using an initial Cr(VI) concentration of 100 mg/L and an adsorbent dose of 0.75 g/L, the study investigated the impact of varying contact time within the 5–90 min range on the removal efficiency of Cr(VI) by BC@PANI composite. The results are visualized in Fig. 6.d, demonstrating that in the initial 5-min period showed a notably rapid increase in the removal efficiency of Cr(VI), reaching a maximum value of 84%. However, following this swift rise, the removal efficiency exhibited a gradual increase, eventually reaching equilibrium over time. This nuanced behavior can be primarily ascribed to the plentiful active sites present in BC@PANI during the initial stage of the adsorption process, enabling the swift adsorption of chromium ions [41]. As time advanced, these active sites were gradually occupied, resulting in a slower rate of efficiency increase and eventual attainment of equilibrium [57]. This observation highlights the intricate dynamics involved in the adsorption process, emphasizing the pivotal role of active site availability in governing the overall adsorption kinetics.

3.2.5 Effect of initial concentration

The influence of the initial concentration of pollutants on the equilibrium adsorption capacity has been widely acknowledged [58]. Hence, in this investigation, varying concentrations of Cr(VI) ranging from 100 to 1000 mg/L have been employed. This has been carried out at three distinct temperatures (298.15 K, 308.15 K, and 318.15 K), while keeping other components constant. In the

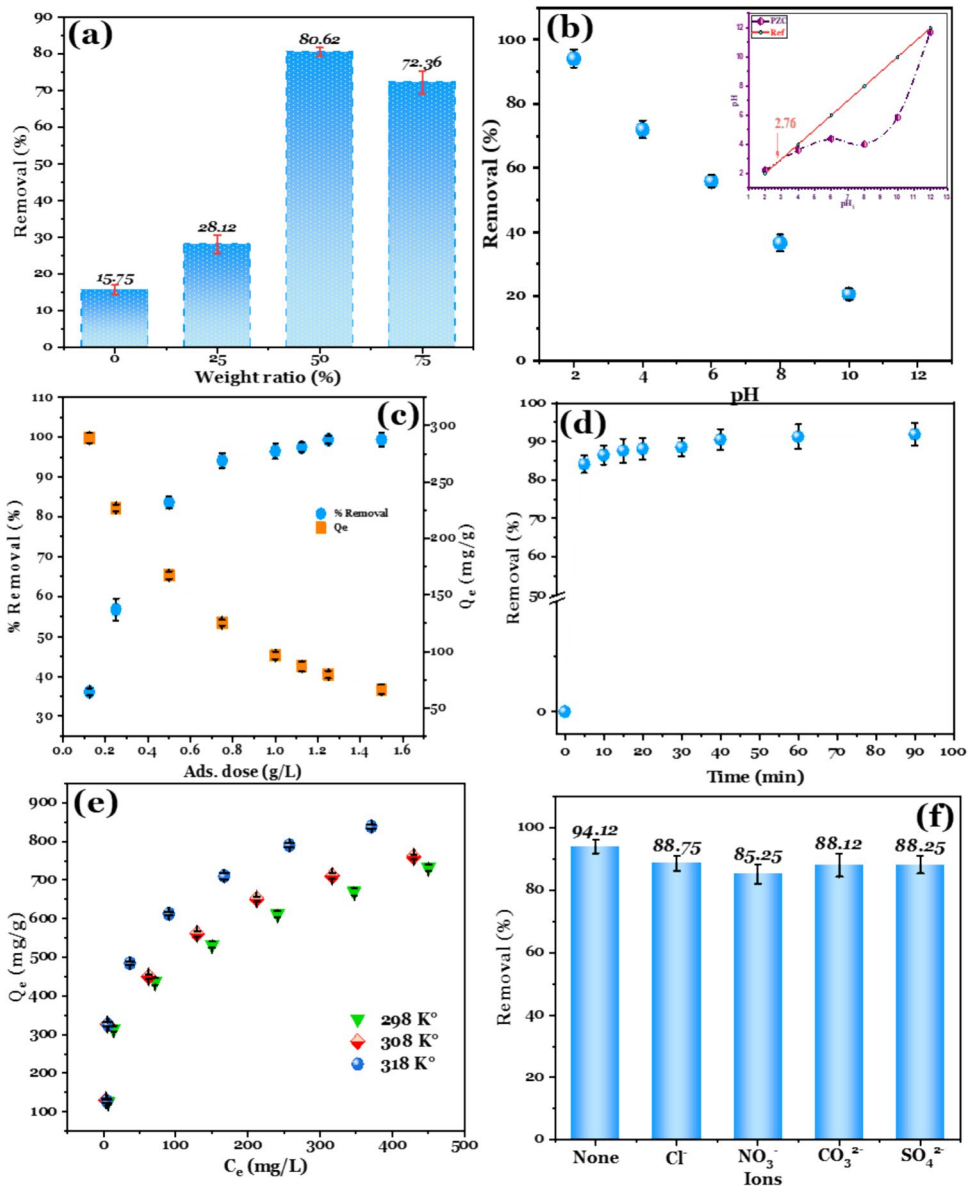

Fig. 6 Effect of several parameters on Cr(VI) elimination, polyaniline weight ratio in the composite **(a)**, solution's pH **(b)**, adsorbent dose **(c)**, Contact time **(d)**, initial Cr(VI) concentration **(e)**, Co-interfering ions **(f)**

investigation of the adsorption process for water treatment using BC@PANI composite, it was observed in Fig. 6.e that the adsorption capacity exhibited a pronounced and sharp increase up to a Cr(VI) equilibrium concentration of 40 ppm. This notable enhancement can be attributed to the escalating concentration disparity between the adsorbent, BC@PANI, and the Cr(VI) solution, thereby amplifying the potential energy-driving force for adsorption [59]. Beyond the 40 ppm threshold, while the adsorption capacity continued to increase, the intensity of this increase diminished. This behavior is elucidated by the occupation of the active sites available on the surface of BC@PANI composite, indicating a saturation phenomenon [46, 60]. At a temperature of 298 K, the adsorption capacity reached 760.10 mg/g for an initial concentration of Cr(VI) ions of 1000 ppm. Furthermore, it was observed that temperature positively influenced the adsorption capacity, as it increased from 732.67 mg/g at 298 K to 838.35 mg/g at 318 K. This temperature-dependent augmentation is indicative of the temperature's favorable impact on the removal efficiency of Cr(VI) ions by BC@PANI composite.

3.2.6 Effect of Co-ions

To ensure relevance to real-world scenarios such as practical wastewater and natural water, we have examined the influence of four common anions, namely Cl^-, NO_3^-, SO^{2-}, and CO_3^{2-}, on the efficacy of BC@PANI composite

in removing Cr(VI). Figure 6.f revealed that the studied anions exerted minimal influence on the overall efficiency of BC@PANI. Among these, NO_3^- demonstrated the most pronounced negative impact on the rate of Cr(VI) elimination, leading to a 9% decrease compared to the blank. The observed result can be linked to the competitive interaction between NO_3^- ions and Cr(VI) ions during the adsorption process on the BC@PANI adsorption sites, leading to a decline in the adsorption efficiency for Cr(VI) ions [61, 62]. However, this implies that the adsorption of Cr(VI) by BC@PANI exhibits a general tendency toward selectivity. This notable selectivity in adsorption is advantageous for the treatment of actual wastewater effluents that contain Cr(VI) compounds [63].

3.3 Adsorption isotherm and kinetic data analysis

3.3.1 Kinetics data

Based on the results from the kinetics models employed in this study, namely PFO [64], PSO [65], Elovich [66], and Intra-particle diffusion (IPD) [67], as depicted in Fig. 7, the adsorption process of Cr(VI) by BC@PANI composite was thoroughly examined. The analysis of the results, as outlined in Table 1, revealed that the PSO model exhibited the best fit, with an impressive R^2 value of 0.9999, surpassing the performance of the PFO model, which yielded a lower R^2 value of 0.8915. This suggests that the adsorption process conforms more closely to the PSO model, as indicated by the nearly identical theoretical adsorption capacity (Qe_{cal}) of 123.00 mg/g and the experimental adsorption capacity (Qe_{exp}) of 122.50 mg/g, which signified that the adsorption process between BC@PANI and Cr(VI) ions is chemical by nature [68, 69]. Furthermore, the application of the Elovich model, with an R^2 value of 0.9767, implied that the Cr(VI) adsorption process was likely a heterogeneous or multi-mechanism phenomenon, thereby highlighting the complexity of the adsorption process [70].

Moreover, the Intra-particle diffusion (IPD) model revealed a multi-stage adsorption process for Cr(VI) by BC@PANI composite. The observed three distinct stages indicated that the adsorption kinetics were not solely governed by the Intra-particle diffusion mechanism [41]. The initial stage, characterized by the highest rate constant (Ki) of 3.4190 $mg.g^{-1}.min^{-1/2}$, exhibited a rapid migration of Cr(VI) molecules from the liquid phase to the external surface of BC@PANI, owing to the driving force and the abundance of unoccupied active sites. Subsequently, the second stage depicted a slower rate, attributed to the penetration of adsorbate Cr(VI) ions into BC@PANI's mesopores, with a corresponding lower rate constant (Ki) of 0.7035 $mg.g^{-1}.min^{-1/2}$. Finally, the third stage signified the attainment of adsorption equilibrium, wherein most binding sites were occupied, and the adsorption process was nearing completion. The non-zero values of Ci at each stage indicated that the Intra-particle diffusion might not have been the sole governing factor driving the removal process of Cr(VI)[71]. These findings collectively underscore the intricate nature of the adsorption process and emphasize the multi-step dynamics involved in the interaction between Cr(VI) ions and BC@PANI composite.

3.3.2 Isotherms modeling

For a comprehensive comprehension of the adsorption mechanism of Cr(VI) ions on the surface of BC@PANI composite, and to gain valuable insights into the surface properties, Langmuir, Freundlich, Temkin, and D-R models were employed across three distinct temperatures (298.15 K, 308.15 K, and 318.15 K). The findings are depicted in Fig. 8 and Table 2.. Langmuir model has the highest R^2 (0.988–0.994) when compared to all the other isotherm models studied, indicating that it is the most well-fitting model to describe Cr(VI) ion adsorption into BC@PANI surface, which suggests that sorption occurs on the surface of BC@PANI at homogenous locations [72], resulting in a mono-layer Cr(VI) adsorption [73]. According to Langmuir model, the theoretical adsorption capacity of BC@PANI composite increases with increasing temperature from 763.36 mg/g at 298.15 K to 877.19 mg/g at 318.15 K, reflecting this process'endothermic nature [74]. Moreover, for the given temperature range (298.15 K-318.15 K), R_L values were found to be 0.1234–0.082, indicating that Cr(VI) is likely to adsorb onto BC@PANI [75].

The Temkin model illustrated in Fig. 8.c emerges as particularly well-suited following Langmuir, boasting correlation coefficients R^2 spanning from 0.9201 to 0.9426. This signifies that the adsorption of Cr(VI) ions and their interaction with BC@PANI are intricately linked to the extent of surface coverage [76]. According to the Dubinin-Radushkevich (D-R) isotherm model described in Fig. 8.d, the calculated activation energy (E) at all the temperatures studied exceeds 40 kJ/mole. This observation reinforces the notion that substantial chemical interactions play a pivotal role in the adsorption process of Cr(VI) by BC@PANI[77]. This finding aligns with the outcomes obtained using the PSO model.

3.4 Adsorbents comparison

BC@PANI composite may demonstrate better adsorption performance when compared with other adsorbents. There have been many studies demonstrating the adsorption of Cr(VI) from water using various adsorbents in the literature. According to Table 3, the material composite had an

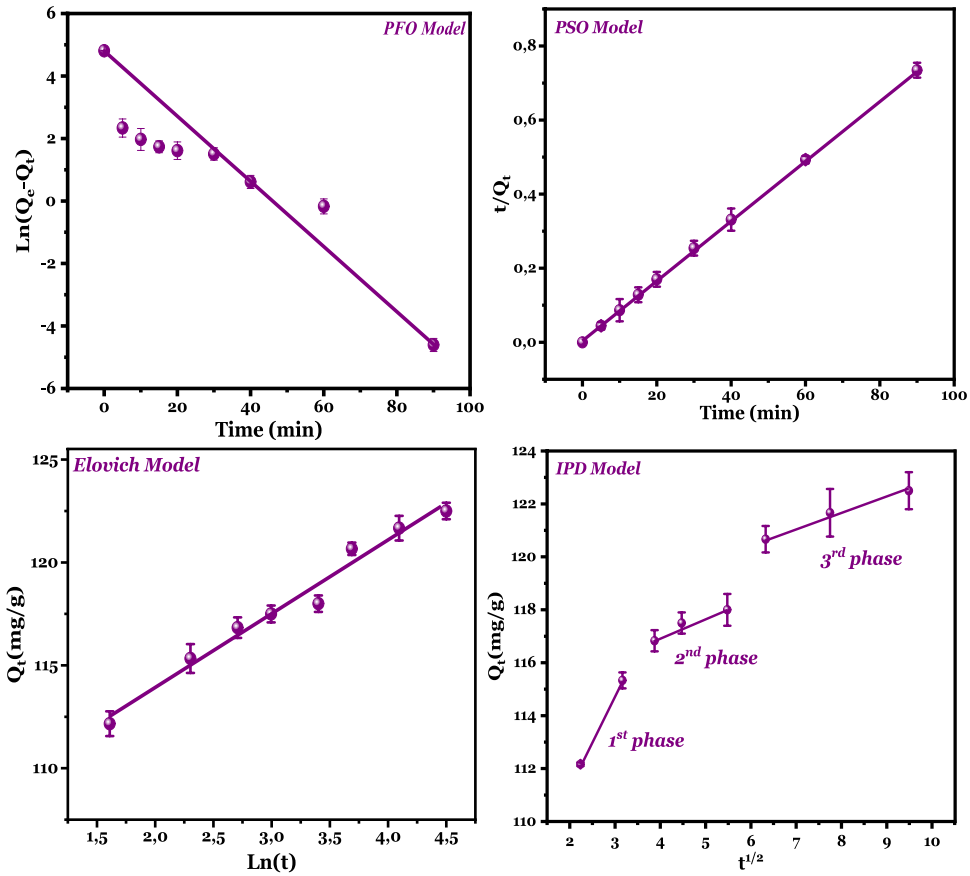

Fig. 7 Kinetics models fit for the adsorption of Cr(VI) onto BC@PANI

excellent maximum uptake capacity (877.19 mg/g) compared to other adsorbents. This suggests that the synthesized adsorbent can be used to efficiently remove Cr(VI). The BC@PANI composite can be recommended as an effective and inexpensive decontamination candidate for Cr(VI)-contaminated wastewater.

The remarkable difference between BC@PANI and other adsorbents can be attributed to several factors. The polyaniline modification introduces a large number of proton-accepting functional groups on the surface of BC, which enhances its effectiveness as an adsorbent and facilitates the reduction of Cr(VI) molecules [45, 47]. Even after reduction, Cr(III) remains adsorbed on the surface of the adsorbent. This could be due to the nitrogen atoms in the BC@PANI composite, which can form coordinate bonds with positively charged Cr(III) ions because of the lone pair electrons on nitrogen [87]. Additionally, the biochar itself can adsorb Cr(III) due to its unique structural properties, such as a large surface area and a highly porous structure [88]. Overall, the combination of electron-rich aromatic ring structures and various nitrogen functional groups of polyaniline, along with the porous architecture of biochar, enables the BC@PANI composite to serve as an exceptional adsorbent for the removal of Cr(VI).

3.5 Thermodynamic study

Three distinct water bath temperatures were employed to examine how Cr(VI) elimination by BC@PANI composite is affected by the temperature of the solution (298.15 K, 308.15 K, and 318.15 K). The initial adsorption capacity at 298.15 K was measured at 498 mg/g, and as the temperature was elevated to 318.15 K, Qe experienced a substantial increase of approximately 55%, ultimately reaching an adsorption capacity of 612.16 mg/g. This remarkable temperature dependence can be elucidated by the consequential decrease in solution viscosity at higher temperatures, facilitating the more efficient diffusion of Cr(VI) molecules into the active sites of BC@PANI composite [75]. As depicted in Table 4, the upward trend in adsorption quantity with increasing temperature highlights the pivotal role of temperature in enhancing the adsorption capacity of BC@PANI for Cr(VI), indicative of the significant influence of temperature on the overall adsorption process. S.M. Ramraj et al. obtained analogous findings regarding the uptake of Cr(VI) by activated charcoal [89].

To investigate the physicochemical effects in the adsorption process between Cr(VI) ions and BC@PANI, a thermodynamic analysis was conducted. The Gibbs free energy (ΔG°), enthalpy (ΔH°), and entropy (ΔS°) were determined

Table 1 Kinetic models and associated parameters for Cr(VI) adsorption onto BC@PANI

Qe_{exp} (mg g^{-1})		122.50	
PFO		Qe_{cal}(mg g^{-1})	34.4680
		K_1 (min^{-1})	0.0817
		R^2	0.8915
PSO		Qe_{cal} (mg g^{-1})	123.0012
		K_2 (g mg^{-1} min^{-1})	0.0125
		R^2	0.9999
Elovic		α	3.6981
		β	0.2796
		R^2	0.9767
IPD	1stStage	C_1(mg g^{-1})	104.5217
		K_i (mg $g^{-1}min^{-1/2}$)	3.4190
		R^2	1.0000
	2nd Stage	C_2 (mg g^{-1})	114.2033
		K_i (mg $g^{-1}min^{-1/2}$)	0.7035
		R^2	0.9492
	3rd Stage	C_3 (mg g^{-1})	117.0880
		K_i (mg $g^{-1}min^{-1/2}$)	0.5760
		R^2	0.9878

from the Van't Hoff plot presented in Fig. S2 using the equations presented in Table S1.

The results presented in Table 4 demonstrate a notable increase in the K_d value, rising from 2821.5 at 298.15 K to 6769.8 at 318.15 K with the elevation of temperature, indicating enhanced efficiency in the adsorption process at elevated temperatures. Furthermore, the positive values of ΔH° (34.30 kJ/mol) and ΔS° (180.46 J/mol/K) confirm the endothermic nature of the Cr(VI) ions adsorption by BC@PANI composite [90], and the augmentation of randomness at the solid–liquid interface [91], respectively. Generally, the manifestation of an exothermic process typically suggests either physisorption or chemisorption, whereas an endothermic process is commonly associated with chemisorption [76]. Moreover, the ΔH° value exceeding 20 kJ/mol affirms that the adsorption process between Cr(VI) ions and BC@PANI is predominantly governed by chemical interactions. Additionally, the negative values of ΔG° across various temperatures indicate the spontaneity and feasibility of the Cr(VI) ions sorption process [92]. Furthermore, the increasing ΔG° value with rising temperature implies that the adsorption of Cr(VI) onto BC@PANI composite becomes more favorable at higher temperatures [44].

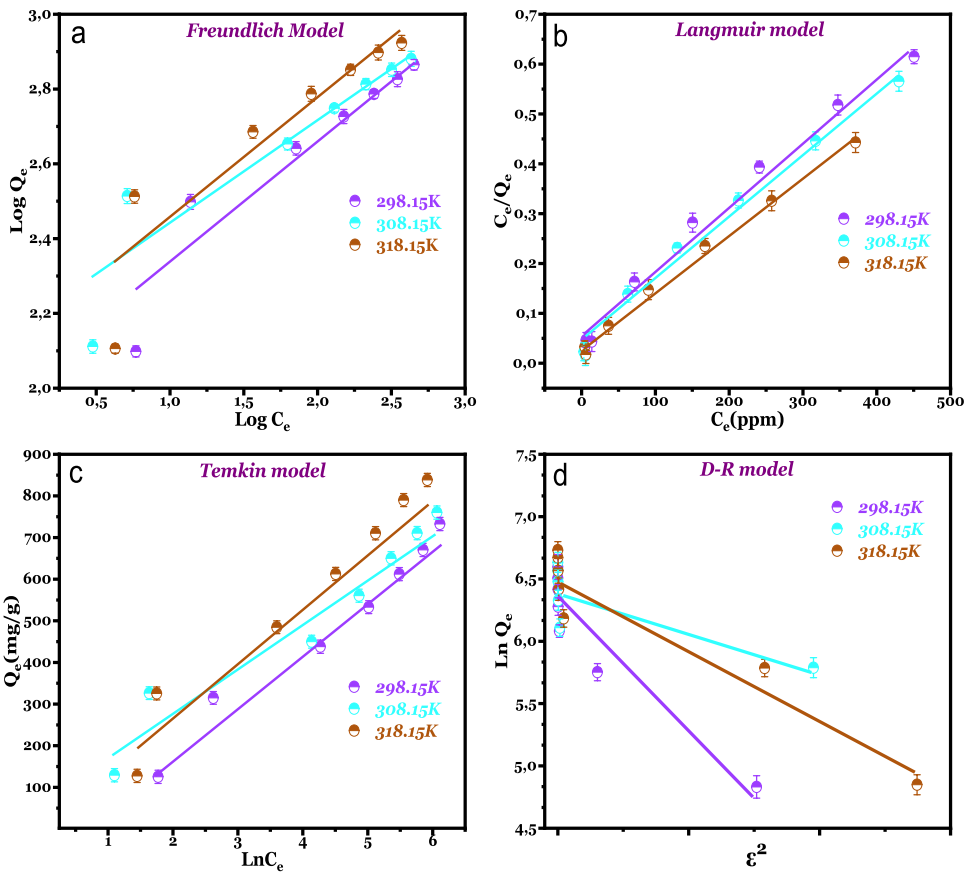

Fig. 8 Freundlich (**a**), Langmuir (**b**), Temkin (**c**) and D-R Isotherm plot of Cr(VI) onto BC@PANI (**d**)

Table 2. The isotherm constants and coefficients for the adsorption of Cr(VI) on BC@PANI

		298.15 K	308.15 K	318.15 K
Qe $_{exp}$ (mg g^{-1})		732,6738	760,1027	838,3543
Langmuir	Q_{max} (mg g^{-1})	763,3587	781,2538	877,1932
	K_L (L/mg)	0,0237	0,0337	0,0371
	R_L	0.1234	0.0899	0.0823
	R^2	0,9877	0,9884	0,9944
Freundlich	K_F (g mg^{-1} min^{-1})	90,3337	135,0892	121,6437
	1/n	0,3516	0,2914	0,3442
	R^2	0,9092	0,8712	0,8556
Temkin	K_T	0,6393	2,3072	1,1653
	B	116,8566	101,3595	128,0868
	b_T(kJ/mol)	21,2125	25,2760	20,6508
	R^2	0,9366	0,9201	0,9426
D-R	Q_D	545,1063	603,2612	665,8071
	B (mol^2/J^2)	1E-05	3E-06	5,7E-06
	E (kJ/mol)	223,5287	405,1294	297,1786
	R^2	0,8926	0,9414	0,9247

3.6 Reusability and regeneration

The reusability of the BC@PANI composite in the adsorption of Chromium (VI) ions was investigated under specific experimental conditions of 100 ppm of Cr(VI) at pH 2. Five cycles were conducted to assess the material's reusability, employing a treatment regimen involving the use of 1 M NaOH as a regenerating agent, followed by redoping with 1 M HCl [93].

Based on the experimental findings presented in Fig. 9.a, the results illustrate that the removal efficiency of Cr(VI) demonstrated a gradual but discernible decline throughout the five cycles. Specifically, after the initial four cycles of adsorption/desorption of Cr(VI), there was a marginal reduction in removal efficiency of approximately 5%, with the efficiency decreasing from 94.75% to 89.13%. However, the most significant decline was observed after the fifth cycle, where the removal efficiency of Cr(VI) notably dropped to 82.5%.

These findings suggest that BC@PANI composite exhibits promising stability for the adsorption of Cr(VI) ions up to the fourth cycle, indicating its potential for multiple applications in the removal of chromium (VI) ions. However, it is crucial to note that beyond the fourth cycle, a considerable decrease in the performance of BC@PANI was observed for the uptake of chromium (VI) ions, implying the necessity for further optimization strategies or regeneration protocols to maintain its adsorption efficiency over prolonged use. These results emphasize the importance of understanding the material's limitations and the need for continued research to enhance its long-term stability and reusability in the adsorption process of Cr(VI) ions.

3.7 Mechanism proposed

To better understand the mechanism of Cr(VI) adsorption onto BC@PANI composite, it is important to note that, as depicted in Fig. 6.b showing the effect of pH, electrostatic interactions primarily govern the Cr(VI)

Table 3 Comparison of adsorption capacity of Cr(VI) ions with other adsorbents

Adsorbent	Qe (mg/g)	Ref
Polyaniline modified biochar	27.30	[44]
Biochar-based iron oxide	24.37	[70]
$ZnCl_2$-modified eucalyptus bark biochar	36.18	[53]
Ball milling biochar iron oxide composites	48.10	[78]
Sugarcane bagasse biochar/nano-iron oxide composite	55.00	[57]
Zinc-doped nickel ferrite-pinecone biochar	29.7	[79]
Nitrogen-doped porous carbon	402.9	[80]
badam-shell biochar	276.6	[81]
Biochar-supported polyaniline	150	[82]
biochar modified by Mg/Al-layered double hydroxides	177.88	[83]
Three-dimensional hierarchical pore biochar	489.66	[84]
Arginine-fuctionalized PANI @ graphitic carbon nitride	204.04	[52]
Polyaniline@magnetic chitosan nanomaterials	186.6	[47]
N, S co-doped porous carbon	382.02	[85]
Zero-valent iron particles immobilized on coconut shell derived carbon	307.8	[86]
BC@PANI	877.19	This study

Table 4 Thermodynamic parameters at different temperatures of Cr(VI) adsorption by BC@PANI

T (K)	Qe (mg g^{-1})	K_d	ΔG° (J mol^{-1})	ΔH° (KJ mol^{-1})	ΔS° (J mol^{-1} K^{-1})
298.15	498.002	2821.530	−19.500	34.303	180.455
308.15	530.201	3475.410	−21.305		
318.15	612.667	6769.797	−23.109		

binding mechanism on the BC@PANI composite. At low pH levels (pH 2), the adsorption capacity of BC@PANI for Cr(VI) ions reaches its maximum. At this pH, the nitrogen atom in PANI donates its lone pair of electrons to acquire positively charged H^+ ions, resulting in the protonation of amine groups such as –NH, $–NH_2$, and –N =. This leads to the formation of positively charged amine and imine groups, which then electrostatically bond with anionic chromate ions like $HCrO^{4-}$ or $Cr_2O_7^{-2}$ [94]. Furthermore, the nitrogen-containing groups in PANI present in the BC@PANI composite act as electron donors, facilitating the reduction of Cr(VI) to Cr(III) ions [41]. Simultaneously, PANI emeraldine salt partially oxidizes to quinoid amines (pernigraniline), which facilitates the removal of the reduced Cr(III) through a complexation reaction [63]. Emphasizing the crucial role of amine functional groups in the adsorption and reduction of Cr(VI). Besides, dissolved Cr(VI) oxyanions can be exchanged with Cl^- ions within the PANI phases. At low pH, $HCrO_4^-$ exhibits a stronger affinity for protonated nitrogen than chloride ions, thereby enhancing the anion exchange process [82]. Figure 9.b provides a graphical overview of the proposed mechanism for Cr(VI) removal from water using the BC@PANI adsorbent.

4 Conclusion

In summary, this study introduces a new approach for enhancing the value of carbonaceous materials obtained from anaerobic digestion residues. It specifically examines the modification of biochar, produced from poultry by-product digestate, to improve the efficient removal of Cr(VI) via a straightforward adsorption process. The PANI-modified biochar demonstrated substantial improvement over the untreated biochar, with effectiveness increasing more than fivefold after modification. Furthermore, the BC@PANI composite stands out for its adsorption capacity, reaching 877.19 mg/g at pH 2 and 318.15 K, surpassing other carbonaceous materials and PANI-based adsorbents. Thermodynamic and pH-dependent studies suggest that the adsorption process is chemisorptive in nature. The proposed mechanism involves electrostatic interactions between Cr(VI) ions and the BC@PANI composite. Importantly, BC@PANI emerges as a pragmatic solution to various environmental challenges, considering its origin from poultry by-product digestate, originally a waste product. This digestate is repurposed after biogas production, demonstrating both waste recovery and energy production. By utilizing BC@PANI in the environmental sector for purifying water contaminated with heavy metals like Cr(VI), this material proves its real-world applicability and practicality.

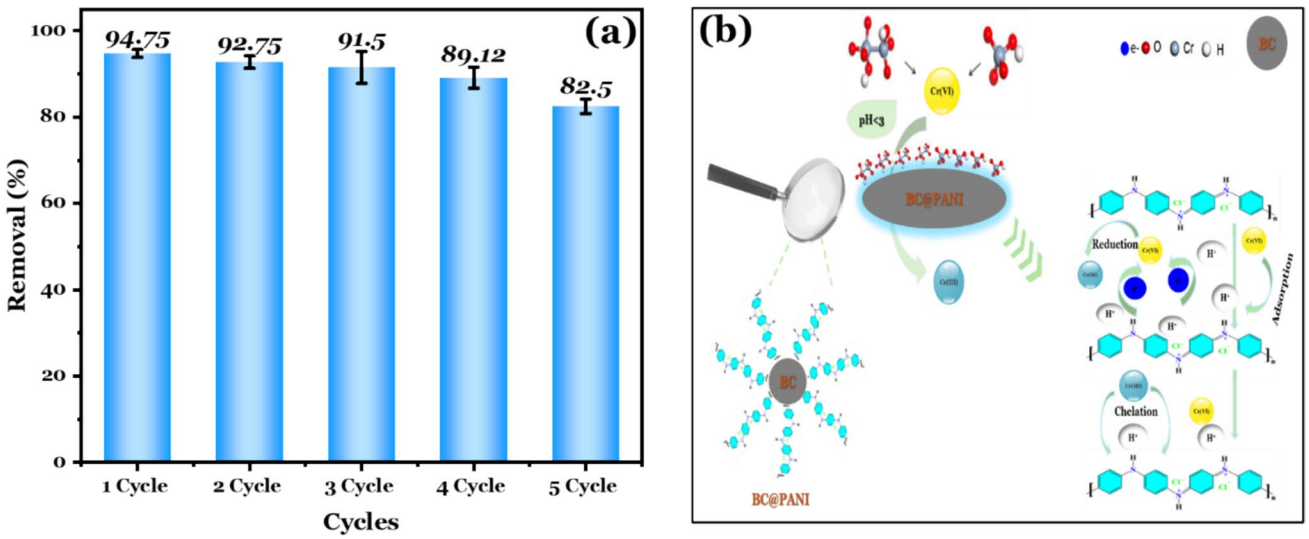

Fig. 9 Recyclability runs of BC@PANI for Cr(VI) elimination **(a)**, Proposal for a tentative mechanism for the adsorption of Cr(VI) and its reduction to Cr(III) **(b)**

Supplementary Information The online version contains supplementary material available athttps://doi.org/10.1007/s42114-025-01345-7.

Acknowledgements We would like to thank the Moroccan Ministry of Higher Education, Scientific Researcher and Innovation and the OCP Foundation who funded this work through the APRD research program. Thanks are due to the project CICECO-Aveiro Institute of Materials, UIDB/50011/2020 (DOI https://doi.org/10.54499/UIDB/50011/2020), UIDP/50011/2020 (DOI https://doi.org/10.54499/UIDP/50011/2020) & LA/P/0006/2020 (DOI https://doi.org/10.54499/LA/P/0006/2020), financed by national funds through the FCT/MCTES (PIDDAC). A.C.E thanks FCT for their research contract funded by National funds (OE), in the scope of the framework contract foreseen in the numbers 4, 5, and 6 of article 23, of the Decree-Law 57/2016, of August 29, changed by Law 57/2017, of July 19 (DL 57/2016/CP1482/CT0007; DOI https://doi.org/10.54499/DL57/2016/CP1482/CT0007).

Author Contribution Ayoub Chaoui: Conceptualization, Methodology, Writing – original draft, Writing – review & editing. Abdelaziz Imgharn Methodology, Writing – original draft, Writing – review & editing. Ana C. Estrada: Conceptualization, Formal analysis. Aboubakr Ben Hamou: Conceptualization, Methodology, Software. Salaheddine Farsad: Conceptualization, Formal analysis, Methodology. Nisrine Nouj: Formal analysis, Investigation. Mohamed Ez-zahery: Resources, Supervision, Validation. Tito Trindade: Validation, Writing – review & editing. Abdallah Albourine: Resources, Investigation, Validation. Noureddine El Alem: Project administration, Supervision, Validation, Writing – review & editing.

Funding This work was supported by the Moroccan Ministry of Higher Education, Scientific Researcher and Innovation and the OCP Foundation who funded this work through the APRD research program.

Data Availability No datasets were generated or analysed during the current study.

Declarations

Conflict of interest The authors declare no competing interests.

References

1. Xie S (2024) Water contamination due to hexavalent chromium and its health impacts: exploring green technology for Cr(VI) remediation. Green Chem Lett Rev 17. https://doi.org/10.1080/17518253.2024.2356614
2. Sharma P, Surendra Pratap S, Sheetal Kishor P, Tong YW (2022) Health hazards of hexavalent chromium (Cr(VI)) and its microbial reduction. Bioengineered 13:4923–4938. https://doi.org/10.1080/21655979.2022.2037273
3. Imgharn A, Laabd M, Naciri Y, Hsini A, Mahir F-Z, Zouggari H, Albourine A (2023) Insights into the performance and mechanism of PANI@Hydroxapatite-Montmorillonite for hexavalent chromium Cr(VI) detoxification. Surfaces Interfaces 36. https://doi.org/10.1016/j.surfin.2022.102568
4. Chang X, Li M, Liu Q, Liu Q, Yao J (2016) Adsorption–reduction of chromium(vi) from aqueous solution by phenol–formaldehyde resin microspheres. RSC Adv 6:46879–46888. https://doi.org/10.1039/C6RA07239A
5. Mallik AK, Moktadir MA, Rahman MA, Shahruzzaman M, Rahman MM (2022) Progress in surface-modified silicas for Cr(VI) adsorption: a review. J Hazard Mater 423:127041. https://doi.org/10.1016/j.jhazmat.2021.127041
6. Chaari I, Fakhfakh E, Medhioub M, Jamoussi F (2019) Comparative study on adsorption of cationic and anionic dyes by smectite rich natural clays. J Mol Struct 1179:672–677. https://doi.org/10.1016/j.molstruc.2018.11.039
7. Laabd M, Imgharn A, Hsini A, Naciri Y, Mobarak M, Szunerits S, Boukherroub R, Albourine A (2022) Efficient detoxification of Cr(VI)-containing effluents by sequential adsorption and reduction using a novel cysteine-doped PANi@faujasite composite: experimental study supported by advanced statistical physics prediction. J Hazard Mater 422:126857. https://doi.org/10.1016/j.jhazmat.2021.126857
8. Farsad S, Amjlef A, Chaoui A, Ben Hamou A, Hamma C, Benafqir M, Jada A, El Alem N (2023) Harnessing a carbon-based material from food waste digestate for dye adsorption: the role of hydrogel beads in enhancing the material stability and regenerative capacity. Mater Adv 4:6599–6611. https://doi.org/10.1039/d3ma00505d
9. Samuel O, Goodness P, Blessing S, Timothy A, Igenepo K (2024) Biomass-derived biochar in wastewater treatment- a circular economy approach. Waste Manag Bull 1:1–14. https://doi.org/10.1016/j.wmb.2023.07.007
10. Wang B, Lan J, Bo C, Gong B, Ou J (2023) Adsorption of heavy metal onto biomass-derived activated carbon: review. RSC Adv 13:4275–4302. https://doi.org/10.1039/d2ra07911a
11. Salam A, Bashir S, Khan I, Hu H (2022) Biochar production and characterization as a measure for effective rapeseed residue and rice straw management: an integrated spectroscopic examination. Biomass Convers Biorefin 12:2687–2696. https://doi.org/10.1007/s13399-020-00820-z
12. Shao Y, Li J, Fang X, Yang Z, Qu Y, Yang M, Tan W, Li G, Wang H (2022) Chemical modification of bamboo activated carbon surface and its adsorption property of simultaneous removal of phosphate and nitrate. Chemosphere 287:132118. https://doi.org/10.1016/j.chemosphere.2021.132118
13. Mahajan P, Jaspal D, Malviya A (2023) Adsorption of dyes using custard apple and wood apple waste : a review. J Indian Chem Soc 100:100948. https://doi.org/10.1016/j.jics.2023.100948
14. Ni B-J, Huang Q-S, Wang C, Ni T-Y, Sun J, Wei W (2019) Competitive adsorption of heavy metals in aqueous solution onto biochar derived from anaerobically digested sludge. Chemosphere 219:351–357. https://doi.org/10.1016/j.chemosphere.2018.12.053
15. Mancuso G, Habchi S, Maraldi M, Valenti F, El H (2024) Bioresource technology comprehensive review of technologies for separate digestate treatment and agricultural valorisation within circular and green economy. Bioresour Technol 409:131252. https://doi.org/10.1016/j.biortech.2024.131252

16. Wang W, Chang J, Lee D (2023) Bioresource technology anaerobic digestate valorization beyond agricultural application : current status and prospects. Bioresour Technol 373:128742. https://doi.org/10.1016/j.biortech.2023.128742
17. Czeka W, Nowak M, Piechota G (2023) Bioresource technology sustainable management and recycling of anaerobic digestate solid fraction by composting: a review. 375. https://doi.org/10.1016/j.biortech.2023.128813
18. Selvaraj PS, Periasamy K, Suganya K, Ramadass K, Muthusamy S, Ramesh P, Bush R, Vincent SGT, Palanisami T (2022) Novel resources recovery from anaerobic digestates: current trends and future perspectives. Crit Rev Environ Sci Technol 52:1915–1999. https://doi.org/10.1080/10643389.2020.1864957
19. Anfar Z, Amedlous A, Ait El Fakir A, Ait Ahsaine H, Zbair M, Lhanafi S, El Haouti R, Jada A, El Alem N (2019) Combined methane energy recovery and toxic dye removal by porous carbon derived from anaerobically modified digestate. ACS Omega 4:9434–9445. https://doi.org/10.1021/acsomega.9b00524
20. Huang W, Xiao S, Zhong H, Yan M, Yang X (2021) Activation of persulfates by carbonaceous materials: a review. Chem Eng J 418:129297. https://doi.org/10.1016/j.cej.2021.129297
21. Wang Y, Song Y, Li N, Liu W, Yan B, Yu Y, Liang L, Chen G, Hou L, Wang S (2022) Tunable active sites on biogas digestate derived biochar for sulfanilamide degradation by peroxymonosulfate activation. J Hazard Mater 421:126794
22. Sabzehmeidani MM, Mahnaee S, Ghaedi M, Heidari H, Roy VAL (2021) Carbon based materials: a review of adsorbents for inorganic and organic compounds. Mater Adv 2:598–627. https://doi.org/10.1039/D0MA00087F
23. Dixit A, Ahammed MM (2023) Bioresource technology reports use of modified biochar for removal of endocrine disrupting compounds from water and wastewater : a review. Bioresour Technol Reports 23:101519. https://doi.org/10.1016/j.biteb.2023.101519
24. Alamin NU, Khan AS, Nasrullah A, Iqbal J, Ullah Z, Din IU, Muhammad N, Khan SZ (2021) Activated carbon-alginate beads impregnated with surfactant as sustainable adsorbent for efficient removal of methylene blue. Int J Biol Macromol 176:233–243. https://doi.org/10.1016/j.ijbiomac.2021.02.017
25. Yan L, Guo W, Huang B, Chen Y, Ren X, Shen Y, Zhou Y, Cheng R, Zhang J, Qiu M, Hu B (2023) Efficient removal of Cr (VI) by the modified biochar with chitosan schiff base and MnFe 2 O 4 nanoparticles : adsorption and mechanism analysis. J Environ Chem Eng 11:109432. https://doi.org/10.1016/j.jece.2023.109432
26. Wu Q, Zhu Y, Duan H, Zhu L, Zhang Y, Xu H, Egun IL, He H (2023) Nano-silicon@ exfoliated graphite/pyrolytic polyaniline composite of a high-performance cathode for lithium storage. Materials (Basel) 16:1584
27. Al-Mur BA, Ansari MO (2023) Silver anchored polyaniline@ molybdenum disulfide nanocomposite (Ag/Pani@ MoS2) for highly efficient ammonia and methanol sensing under ambient conditions: a mechanistic approach. Nanomaterials 13:828
28. Hsini A, Naciri Y, Benafqir M, Ajmal Z, Aarab N, Laabd M, Navío JA, Puga F, Boukherroub R, Bakiz B, Albourine A (2021) Facile synthesis and characterization of a novel 1,2,4,5-benzene tetracarboxylic acid doped polyaniline@zinc phosphate nanocomposite for highly efficient removal of hazardous hexavalent chromium ions from water. J Colloid Interface Sci 585:560–573. https://doi.org/10.1016/j.jcis.2020.10.036
29. Amjlef A, Farsad S, Ait A, Fakir E, El A, El S, Et-taleb S, El N (2023) Polyaniline-encapsulated quartz sand as an adsorbent composite for Orange G dye removal from aqueous solution: experimental and computational study. Ceram Int. https://doi.org/10.1016/j.ceramint.2022.12.293
30. Kumar A, Kim JH, Ranjan P, Metcalfe MG, Cao W, Mishina M, Gangappa S, Guo Z, Boyden ES, Zaki S, York I, García-Sastre A, Shaw M, Sambhara S (2017) Influenza virus exploits tunneling nanotubes for cell-to-cell spread. Sci Rep 7:40360. https://doi.org/10.1038/srep40360
31. Gong K, Hu Q, Xiao Y, Cheng X, Liu H, Wang N, Qiu B, Guo Z (2018) Triple layered core–shell ZVI@carbon@polyaniline composite enhanced electron utilization in Cr(vi) reduction. J Mater Chem A 6:11119–11128. https://doi.org/10.1039/C8TA03066A
32. Hajjaoui H, Soufi A, Khnifira M, Abdennouri M (2023) Mono and binary mixture removal of eriochrome black T and Cr (VI) from water by SiO 2 / polyaniline composite. Mater Chem Phys 296:127220. https://doi.org/10.1016/j.matchemphys.2022.127220
33. Zhang B, Hu R, Sun D, Wu T, Li Y (2018) Fabrication of chitosan/magnetite-graphene oxide composites as a novel bioadsorbent for adsorption and detoxification of Cr(VI) from aqueous solution. Sci Rep 8:1–12. https://doi.org/10.1038/s41598-018-33925-7
34. Hsini A, Naciri Y, Laabd M, Bouziani A, Navío JA, Puga F, Boukherroub R, Lakhmiri R, Albourine A (2021) Journal of Environmental Chemical Engineering Development of a novel PANI @ WO 3 hybrid composite and its application as a promising adsorbent for Cr (VI) ions removal. J Environ Chem Eng 9:105885. https://doi.org/10.1016/j.jece.2021.105885
35. Roy H, Prantika TR, Riyad MH, Paul S, Islam MS (2022) Synthesis, characterizations, and RSM analysis of Citrus macroptera peel derived biochar for textile dye treatment, South African. J Chem Eng 41:129–139. https://doi.org/10.1016/j.sajce.2022.05.008
36. Dai J, Meng X, Zhang Y, Huang Y (2020) Bioresource technology effects of modification and magnetization of rice straw derived biochar on adsorption of tetracycline from water. Bioresour Technol 311:123455. https://doi.org/10.1016/j.biortech.2020.123455
37. He X, Neng Hong Z, Yong Shi R, Qi Cui J, Wei Lai H, Long Lu H, Kou Xu R (2022) The effects of H2O2- and HNO3/H2SO4-modified biochars on the resistance of acid paddy soil to acidification. Environ Pollut 293:118588. https://doi.org/10.1016/j.envpol.2021.118588
38. Huang S, Wang T, Chen K, Mei M, Liu J, Li J (2020) Engineered biochar derived from food waste digestate for activation of peroxymonosulfate to remove organic pollutants. Waste Manag 107:211–218. https://doi.org/10.1016/j.wasman.2020.04.009
39. Liu J, Jia H, Mei M, Wang T, Chen S, Li J (2022) Efficient degradation of diclofenac by digestate-derived biochar catalyzed peroxymonosulfate oxidation: performance, machine learning prediction, and mechanism. Process Saf Environ Prot 167:77–88. https://doi.org/10.1016/j.psep.2022.09.007
40. Khalili S, Khoshandam B, Jahanshahi M (2016) RSC Advances Synthesis of activated carbon / polyaniline nanocomposites for enhanced CO 2 adsorption †. RSC Adv 6:35692–35704. https://doi.org/10.1039/C6RA00884D
41. Kumari B, Tiwary RK, Yadav M (2023) Effect of poly-aniline coated iron ore mining waste (PANI @ IOMW) as efficient adsorbent on mitigation of Cr (VI) from aqueous solution: Experimental and chem. Eng Res Des 190:434–450. https://doi.org/10.1016/j.cherd.2022.12.008
42. Bai M, Chai Y, Chen A, Yuan J, Shang C, Peng L, Peng C (2023) Enhancing cadmium removal efficiency through spinel ferrites modified biochar derived from agricultural waste straw. J Environ Chem Eng 11:109027. https://doi.org/10.1016/j.jece.2022.109027
43. Verma CJ, Kumar A, Pal S, Sinha S, Singh AK, Jaiswal A, Prakash R (2020) Polyaniline stabilized activated carbon from Eichhornia Crassipes : potential charge storage material from biowaste. Renew Energy 162:2285–2296. https://doi.org/10.1016/j.renene.2020.09.135
44. Tripathy S, Sahu S, Patel RK, Panda RB, Kar PK (2021) Efficient removal of Cr(VI) by polyaniline modified biochar from date (Phoenix dactylifera) seed. Groundw Sustain Dev. 15:100653. https://doi.org/10.1016/j.gsd.2021.100653

45. Yu L, Li D, Xu Z, Zheng S (2023) Chemosphere polyaniline coated Pt / CNT as highly stable and active catalyst for catalytic hydrogenation reduction of Cr (VI). 310. https://doi.org/10.1016/j.chemosphere.2022.136685
46. Hsini A, Essekri A, Aarab N, Laabd M (2020) Elaboration of novel polyaniline @ Almond shell biocomposite for effective removal of hexavalent chromium ions and Orange G dye from aqueous solutions.
47. Lei C, Wang C, Chen W, He M, Huang B (2020) Polyaniline@ magnetic chitosan nanomaterials for highly efficient simultaneous adsorption and in-situ chemical reduction of hexavalent chromium: removal efficacy and mechanisms. Sci Total Environ 733:139316. https://doi.org/10.1016/j.scitotenv.2020.139316
48. Hsini A, Naciri Y, Laabd M, El Ouardi M, Ajmal Z, Lakhmiri R, Boukherroub R, Albourine A (2020) Synthesis and characterization of arginine-doped polyaniline/walnut shell hybrid composite with superior clean-up ability for chromium (VI) from aqueous media: Equilibrium, reusability and process optimization. J Mol Liq 316:113832. https://doi.org/10.1016/j.molliq.2020.113832
49. Yao X, Ji L, Guo J, Ge S, Lu W, Cai L, Wang Y, Song W, Zhang H (2020) Magnetic activated biochar nanocomposites derived from wakame and its application in methylene blue adsorption. Bioresour Technol 302:122842. https://doi.org/10.1016/j.biortech.2020.122842
50. Zhu K, Gao Y, Tan X, Chen C (2016) Polyaniline modified Mg/Al layered double hydroxide composites and their application in efficient removal of Cr(VI). ACS Sustain Chem Eng. https://doi.org/10.1021/acssuschemeng.6b00922
51. Kumari B, Tiwary RK, Yadav M (2022) Non linear regression analysis and RSM modeling for removal of Cr(VI) from aqueous solution using PANI@WH composites. Mater Chem Phys 290. https://doi.org/10.1016/j.matchemphys.2022.126457
52. Mahir F, Zouggari H, Imgharn A, Hsini A, Aarab N, Laabd M, Aït A, El H, Albourine A (2023) Diamond & Related Materials Facile elaboration of arginine-functionalized PANI @ graphitic carbon nitride for efficient removal of hexavalent chromium. Diam Relat Mater 136:109963. https://doi.org/10.1016/j.diamond.2023.109963
53. Yusuff AS, Lala MA, Thompson-Yusuff KA, Babatunde EO (2022) ZnCl2-modified eucalyptus bark biochar as adsorbent: preparation, characterization and its application in adsorption of Cr(VI) from aqueous solutions, South African. J Chem Eng 42:138–145. https://doi.org/10.1016/j.sajce.2022.08.002
54. Dong Y, Liu Q, Gao T, Zhang X, Yao J, Zhang C (2022) Tannin-diethylenetriamine based adsorbents with exceptional adsorption capacity of Chromium (VI) in aqueous solution. J Taiwan Instit Chem Eng 141. https://doi.org/10.1016/j.jtice.2022.104603
55. Shakya A, Agarwal T (2019) Removal of Cr(VI) from water using pineapple peel derived biochars: adsorption potential and re-usability assessment. J Mol Liq 293:111497. https://doi.org/10.1016/j.molliq.2019.111497
56. Shakya A, Vithanage M, Agarwal T (2022) Influence of pyrolysis temperature on biochar properties and Cr(VI) adsorption from water with groundnut shell biochars: mechanistic approach. Environ Res 215:114243. https://doi.org/10.1016/j.envres.2022.114243
57. Bai L, Su X, Feng J, Ma S (2021) Preparation of sugarcane bagasse biochar/nano-iron oxide composite and mechanism of its Cr(VI) adsorption in water. J Clean Prod 320. https://doi.org/10.1016/j.jclepro.2021.128723
58. Aliabadi M, Khazaei I, Fakhraee H, Mousavian MTH (2012) Hexavalent chromium removal from aqueous solutions by using low-cost biological wastes : equilibrium and kinetic studies. 319–326. https://doi.org/10.1007/s13762-012-0045-7
59. Yang Y, Zhang Y, Wang G, Yang Z, Xian J, Yang Y, Li T, Pu Y, Jia Y, Li Y, Cheng Z, Zhang S, Xu X (2021) Adsorption and reduction of Cr(VI) by a novel nanoscale FeS/chitosan/biochar composite from aqueous solution. J Environ Chem Eng 9:105407. https://doi.org/10.1016/j.jece.2021.105407
60. Amjlef A, Farsad S, Chaoui A, Ben Hamou A, Ezzahery M, Et-Taleb S, El Alem N (2023) Effective adsorption of Orange G dye using chitosan cross-linked by glutaraldehyde and reinforced with quartz sand. Int J Biol Macromol 239:124373. https://doi.org/10.1016/j.ijbiomac.2023.124373
61. Shi X, Qiao Y, An X, Tian Y, Zhou H (2020) High-capacity adsorption of Cr(VI) by lignin-based composite: characterization, performance and mechanism. Int J Biol Macromol 159:839–849. https://doi.org/10.1016/j.ijbiomac.2020.05.130
62. Tie J, Li W, Liu H, Huang K, Mi X, Wei M, Hou L (2023) Efficient adsorption and reduction of Cr (VI) by a novel polyaniline modified magnetic iron-based waterworks sludge from aqueous solution. Chem Eng J 451:137673. https://doi.org/10.1016/j.cej.2022.137673
63. Hsini A, Benafqir M, Naciri Y, Laabd M, Albourine A (2021) Synthesis of an arginine-functionalized polyaniline @ FeOOH composite with high removal performance of hexavalent chromium ions from water : adsorption behavior, regeneration and process capability studies. Colloids Surf A Physicochem Eng Asp 617:126274. https://doi.org/10.1016/j.colsurfa.2021.126274
64. Jabar JM, Odusote YA, Ayinde YT, Yılmaz M (2022) African almond (Terminalia catappa L) leaves biochar prepared through pyrolysis using H3PO4 as chemical activator for sequestration of methylene blue dye. Results Eng 14:100385. https://doi.org/10.1016/j.rineng.2022.100385
65. Nnadozie EC, Ajibade PA (2020) Adsorption, kinetic and mechanistic studies of Pb(II) and Cr(VI) ions using APTES functionalized magnetic biochar. Microporous Mesoporous Mater 309:110573. https://doi.org/10.1016/j.micromeso.2020.110573
66. Pei T, Shi F, Hou D, Yang F, Lu , Liu C, Lin X, Lu Y, Zheng Z, Zheng Y (2023) Enhanced adsorption of phenol from aqueous solution by KOH combined Fe-Zn bimetallic oxide co-pyrolysis biochar : fabrication , performance , and mechanism. Bioresour Technol 388. https://doi.org/10.1016/j.biortech.2023.129746
67. Goswami R, Dey AK (2022) Use of anionic surfactant-modified activated carbon for efficient adsorptive removal of crystal violet dye. Adsorpt Sci Technol 2022:2357242. https://doi.org/10.1155/2022/2357242
68. Zhang B, Wu Y, Cha L (2020) Removal of methyl orange dye using activated biochar derived from pomelo peel wastes: performance, isotherm, and kinetic studies. J Dispers Sci Technol 41:125–136. https://doi.org/10.1080/01932691.2018.1561298
69. Sirajudheen P, Karthikeyan P, Vigneshwaran S, Meenakshi S (2020) Synthesis and characterization of La(III) supported carboxymethylcellulose-clay composite for toxic dyes removal: evaluation of adsorption kinetics, isotherms and thermodynamics. Int J Biol Macromol 161:1117–1126. https://doi.org/10.1016/j.ijbiomac.2020.06.103
70. Dong FX, Yan L, Zhou XH, Huang ST, Liang JY, Zhang WX, Guo ZW, Guo PR, Qian W, Kong LJ, Chu W, Diao ZH (2021) Simultaneous adsorption of Cr(VI) and phenol by biochar-based iron oxide composites in water: performance, kinetics and mechanism. J Hazard Mater 416:125930. https://doi.org/10.1016/j.jhazmat.2021.125930
71. Nchoe OB, Sanni SO, Viljoen EL, Pholosi A, Pakade VE (2023) Surfactant-modified macadamia nutshell for enhancement of methylene blue dye adsorption from aqueous media. Case Stud Chem Environ Eng 8:100357. https://doi.org/10.1016/j.cscee.2023.100357
72. Yin G, Song X, Tao L, Sarkar B, Sarmah AK, Zhang W, Lin Q, Xiao R, Liu Q, Wang H (2020) Novel Fe-Mn binary oxide-biochar

as an adsorbent for removing Cd(II) from aqueous solutions. Chem Eng J 389:124465. https://doi.org/10.1016/j.cej.2020.124465
73. Karaman C, Karaman O, Show PL, Karimi-Maleh H, Zare N (2022) Congo red dye removal from aqueous environment by cationic surfactant modified-biomass derived carbon: equilibrium, kinetic, and thermodynamic modeling, and forecasting via artificial neural network approach. Chemosphere 290:133346. https://doi.org/10.1016/j.chemosphere.2021.133346
74. Dehmani Y, Franco DSP, Georgin J, Lamhasni T, Brahmi Y, Oukhrib R, Ben Youcef H, Sadik A (2023) Towards experimental and theoretical understanding of the adsorption behavior of phenol on a new activated carbon prepared from oak wood. J Water Process Eng 54:103936. https://doi.org/10.1016/j.jwpe.2023.103936
75. Ding H, Zhang Z, Li Y, Ding L, Sun D, Dong Z (2022) Fabrication of novel Fe/Mn/N co-doped biochar and its enhanced adsorption for bisphenol a based on π–π electron donor–acceptor interaction. Bioresour Technol 364:128018. https://doi.org/10.1016/j.biortech.2022.128018
76. Ebisike K, Elvis Okoronkwo A, Kanayo Alaneme K, Jeremiah Akinribide O (2023) Thermodynamic study of the adsorption of Cd2+ and Ni2+ onto chitosan – silica hybrid aerogel from aqueous solution. Res Chem 5:100730. https://doi.org/10.1016/j.rechem.2022.100730
77. Yan Y, Qi F, Zhang L, Zhang P, Li Q (2022) Enhanced Cd adsorption by red mud modified bean-worm skin biochars in weakly alkali environment. Sep Purif Technol 297:121533. https://doi.org/10.1016/j.seppur.2022.121533
78. Zou H, Zhao J, He F, Zhong Z, Huang J, Zheng Y, Zhang Y, Yang Y, Yu F, Bashir MA, Gao B (2021) Ball milling biochar iron oxide composites for the removal of chromium (Cr(VI)) from water: performance and mechanisms. J Hazard Mater 413:125252. https://doi.org/10.1016/j.jhazmat.2021.125252
79. Masuku M, Nure JF, Atagana HI, Hlongwa N, Nkambule TTI (2024) Advancing the development of nanocomposite adsorbent through zinc-doped nickel ferrite-pinecone biochar for removal of chromium (VI) from wastewater. Sci Total Environ 908:168136. https://doi.org/10.1016/j.scitotenv.2023.168136
80. Liang H, Sun R, Song B, Sun Q, Peng P, She D (2020) Preparation of nitrogen-doped porous carbon material by a hydrothermal-activation two-step method and its high-efficiency adsorption of Cr(VI). J Hazard Mater 387:121987. https://doi.org/10.1016/j.jhazmat.2019.121987
81. Jia X, Zhang Y, He Z, Chang F, Zhang H, Wågberg T, Hu G (2021) Mesopore-rich badam-shell biochar for efficient adsorption of Cr(VI) from aqueous solution. J Environ Chem Eng 9:105634. https://doi.org/10.1016/j.jece.2021.105634
82. Herath A, Reid C, Perez F, Pittman CU, Mlsna TE (2021) Biochar-supported polyaniline hybrid for aqueous chromium and nitrate adsorption. J Environ Manage 296:113186. https://doi.org/10.1016/j.jenvman.2021.113186
83. Li X, Shi Z, Zhang J, Gan T, Xiao Z (2023) Aqueous Cr(VI) removal performance of an invasive plant-derived biochar modified by Mg/Al-layered double hydroxides. Colloid Interface Sci Commun 53. https://doi.org/10.1016/j.colcom.2023.100700
84. Kuang Q, Liu K, Wang Q, Chang Q (2023) Three-dimensional hierarchical pore biochar prepared from soybean protein and its excellent Cr(VI) adsorption. Sep Purif Technol 304:122295. https://doi.org/10.1016/j.seppur.2022.122295
85. Yang X, Wang B, Zhang P, Song X, Cheng F (2024) Adsorption and reduction of Cr(VI) by N, S co-doped porous carbon from sewage sludge and low-rank coal: combining experiments and theoretical calculations. Sci Total Environ 912:169265. https://doi.org/10.1016/j.scitotenv.2023.169265
86. Yu P, Tan J, Wang Z, Zhang C, Wang Q, Zhu K, Peng C, Xiao X, Huang W (2024) Enhanced electron transfer pathway of zero-valent iron particles immobilized on coconut shell derived carbon for prolonged Cr(VI) removal. Colloids Surfaces A Physicochem Eng Asp 682:132863. https://doi.org/10.1016/j.colsurfa.2023.132863
87. Tang L, Fang Y, Pang Y, Zeng G, Wang J, Zhou Y (2014) Synergistic adsorption and reduction of hexavalent chromium using highly uniform polyaniline – magnetic mesoporous silica composite. Chem Eng J 254:302–312. https://doi.org/10.1016/j.cej.2014.05.119
88. Murad HA, Ahmad M, Bundschuh J, Hashimoto Y, Zhang M, Sarkar B, Ok YS (2022) A remediation approach to chromium-contaminated water and soil using engineered biochar derived from peanut shell. Environ Res 204:112125. https://doi.org/10.1016/j.envres.2021.112125
89. Ramraj SM, Kubaib A, Imran PM, Thirupathy MK (2023) Utilizing Sida Acuta leaves for low-cost adsorption of chromium (VI) heavy metal with activated charcoal. J Hazard Mater Adv 11:100338. https://doi.org/10.1016/j.hazadv.2023.100338
90. Jawad AH, Ezzuldin S, Saber M, Saud A, Reghioua A, Alothman ZA, Wilson LD (2022) mesoporous activated carbon from mangosteen (Garcinia mangostana) peels by H 3 PO 4 assisted microwave : optimization , characterization , and adsorption mechanism for methylene blue dye removal. Diamond & related materials 129. https://doi.org/10.1016/j.diamond.2022.109389
91. Yin G, Chen X, Sarkar B, Bolan NS, Wei T, Zhou H, Wang H (2023) Co-adsorption mechanisms of Cd (II) and As (III) by an Fe-Mn binary oxide biochar in aqueous solution. Chem Eng J 466:143199
92. Kumar Prajapati A, Kumar Mondal M (2022) Green synthesis of Fe3O4-onion peel biochar nanocomposites for adsorption of Cr(VI), methylene blue and congo red dye from aqueous solutions. J Mol Liq 349:118161. https://doi.org/10.1016/j.molliq.2021.118161
93. Imgharn A, Anchoum L, Hsini A, Naciri Y, Laabd M, Mobarak M, Aarab N, Bouziani A, Szunerits S, Boukherroub R, Lakhmiri R, Albourine A (2022) Effectiveness of a novel polyaniline@Fe-ZSM-5 hybrid composite for Orange G dye removal from aqueous media: experimental study and advanced statistical physics insights. Chemosphere 295:133786. https://doi.org/10.1016/j.chemosphere.2022.133786
94. Kumari B, Tiwary RK, Yadav M (2022) Non linear regression analysis and response surface modeling for Cr (VI) removal from aqueous solution using poly-aniline coated sugarcane bagasse (PANI @ SB) composites as an adsorbent. Surface Interfaces 29:101729. https://doi.org/10.1016/j.surfin.2022.101729